

Understanding electron heat flux signatures in the solar wind

Article

Published Version

Pagel, C., Crooker, N.U., Larson, D.E., Kahler, S.W. and Owens, M.J. ORCID: <https://orcid.org/0000-0003-2061-2453> (2005) Understanding electron heat flux signatures in the solar wind. *Journal of Geophysical Research*, 110. A01103. ISSN 0148-0227 doi: 10.1029/2004JA010767 Available at <https://centaur.reading.ac.uk/5835/>

It is advisable to refer to the publisher's version if you intend to cite from the work. See [Guidance on citing](#).

To link to this article DOI: <http://dx.doi.org/10.1029/2004JA010767>

Publisher: American Geophysical Union

All outputs in CentAUR are protected by Intellectual Property Rights law, including copyright law. Copyright and IPR is retained by the creators or other copyright holders. Terms and conditions for use of this material are defined in the [End User Agreement](#).

www.reading.ac.uk/centaur

CentAUR

Central Archive at the University of Reading

Reading's research outputs online

Understanding electron heat flux signatures in the solar wind

C. Pagel,¹ N. U. Crooker,¹ D. E. Larson,² S. W. Kahler,³ and M. J. Owens¹

Received 30 August 2004; revised 26 October 2004; accepted 1 November 2004; published 8 January 2005.

[1] Suprathermal electrons ($E > 80$ eV) carry heat flux away from the Sun. Processes controlling the heat flux are not well understood. To gain insight into these processes, we model heat flux as a linear dependence on two independent parameters: electron number flux and electron pitch angle anisotropy. Pitch angle anisotropy is further modeled as a linear dependence on two solar wind components: magnetic field strength and plasma density. These components show no correlation with number flux, reinforcing its independence from pitch angle anisotropy. Multiple linear regression applied to 2 years of Wind data shows good correspondence between modeled and observed heat flux and anisotropy. The results suggest that the interplay of solar wind parameters and electron number flux results in distinctive heat flux dropouts at heliospheric features like plasma sheets but that these parameters continuously modify heat flux. This is inconsistent with magnetic disconnection as the primary cause of heat flux dropouts. Analysis of fast and slow solar wind regimes separately shows that electron number flux and pitch angle anisotropy are equally correlated with heat flux in slow wind but that number flux is the dominant correlative in fast wind. Also, magnetic field strength correlates better with pitch angle anisotropy in slow wind than in fast wind. The energy dependence of the model fits suggests different scattering processes in fast and slow wind.

Citation: Pagel, C., N. U. Crooker, D. E. Larson, S. W. Kahler, and M. J. Owens (2005), Understanding electron heat flux signatures in the solar wind, *J. Geophys. Res.*, 110, A01103, doi:10.1029/2004JA010767.

1. Introduction

[2] Electrons are responsible for transporting most of the heat flux away from the Sun due to their high mobility. The rate at which heat flux drops off with radial distance from the Sun implies some in-transit scattering processes [Pilipp *et al.*, 1990; Scime *et al.*, 1994; Hammond *et al.*, 1996]. Hence to better understand the heliospheric transportation of solar heat flux, we require a thorough understanding of the electron heat flux signatures in the solar wind. Moreover, a better knowledge of processes regulating heliospheric electron heat flux would provide important information regarding the amount of disconnected magnetic flux in the heliosphere, which should give relatively clear cut dropout signatures in the solar wind [e.g., McComas *et al.*, 1989; Crooker *et al.*, 2003]. If, instead, heat flux dropouts are part of a continuous heat flux regulating process, then they are unlikely to be signatures of magnetic disconnection.

[3] The electron velocity distribution can be split into a core thermal distribution and a hot, suprathermal distribution with the breakpoint between the two placed at 50–

100 eV [Feldman *et al.*, 1975, 1976a, 1976b]. The hot electrons are sometimes called the “halo” [Feldman *et al.*, 1975; Pilipp *et al.*, 1987a; Ogilvie *et al.*, 1999]. Further, the suprathermal electrons can be considered as consisting of an isotropic halo and a narrow beam, the strahl, aligned with the heliospheric magnetic field [Feldman *et al.*, 1978; Pilipp *et al.*, 1987a, 1987b] (see also Gosling *et al.* [2004] for a current discussion on these definitions). In this paper, “halo” electrons refer exclusively to the isotropic part of the suprathermal electron distributions.

[4] Heat flux often drops at and near sector boundaries [Pilipp *et al.*, 1990; McComas *et al.*, 1989; Fitzenreiter and Ogilvie, 1992; Crooker *et al.*, 2003]. This could be due to either magnetic field disconnection from the Sun [McComas *et al.*, 1989] or enhanced scattering. Most heat flux dropouts are not apparent in the highest-energy electrons, favoring scattering over disconnection [Lin and Kahler, 1992; Fitzenreiter and Ogilvie, 1992] and consistent with observations of the pitch angle distributions isotropizing at and near sector boundaries [Pilipp *et al.*, 1987a, 1987b, 1990; Ogilvie *et al.*, 1999; Crooker *et al.*, 2003]. Sector boundaries are often surrounded by the heliospheric plasma sheet, characterized by low magnetic field magnitude and high plasma density [Winterhalter *et al.*, 1994; Crooker *et al.*, 2004]. Isotropic pitch angle distributions have been observed in these high-beta plasma sheets as well as in sheets not associated with sector boundaries [Crooker *et al.*, 2003, 2004] and in regions of low magnetic field intensity [Chisham *et al.*, 2000; Zurbuchen *et al.*, 2001]. Away from sector boundaries, pitch angle distributions are more anisotropic [Pilipp *et al.*, 1987a, 1987b, 1990; Ogilvie *et al.*,

¹Center for Space Physics, Boston University, Boston, Massachusetts, USA.

²Space Science Laboratory, University of California, Berkeley, California, USA.

³Air Force Research Laboratory, Hanscom Air Force Base, Massachusetts, USA.

1999], correlated with magnetic field magnitude [Pilipp *et al.*, 1990; Scime *et al.*, 1994], and sometimes anticorrelated with plasma density [Pilipp *et al.*, 1990; Ogilvie *et al.*, 1999, 2000].

[5] Several scattering mechanisms have been proposed to account for the regulation of electron heat flux in local solar wind plasma. Alfvén [Feldman *et al.*, 1976b] and whistler wave instabilities [Feldman *et al.*, 1975; Scime *et al.*, 1994] have been suggested and later discounted [McComas *et al.*, 1989; Scime *et al.*, 1994, 1999, 2001]. Coulomb scattering and ion acoustic turbulence have also been discounted as primary scattering mechanisms [Pilipp *et al.*, 1987b; Scime *et al.*, 1994], although Ogilvie *et al.* [2000] still suggest that some coulomb scattering occurs in regions of high plasma density. Large magnetic field fluctuations in regions of low magnetic field strength could be partially responsible for scattering suprathermal electrons [Zurbuchen *et al.*, 2001; Mullan *et al.*, 2003], while low levels of magnetic field fluctuations correspond to highly anisotropic pitch angle distributions [Ogilvie *et al.*, 2000].

[6] Electron heat flux Q is dominated by the number flux F_H of the suprathermal electrons rather than the core electrons and can be phenomenologically described as the bulk drift $\Delta\mathbf{V}_H$ of the hot electrons relative to the total electron distribution, expressed as $\mathbf{Q} \sim F_H \Delta\mathbf{V}_H$ [Feldman *et al.*, 1975; Scime *et al.*, 1994]. Hence the heat flux should vary with both F_H and $\Delta\mathbf{V}_H$. When the suprathermal electron velocity vector is narrowly aligned with the local magnetic field (i.e., its component along the magnetic field direction is large), $|\Delta\mathbf{V}_H|$ will be high. This corresponds to anisotropic electron pitch angle distributions, and so the anisotropy of the pitch angle distributions should also contribute to the observed value of the heat flux. Pilipp *et al.* [1987a, 1990], Zurbuchen *et al.* [2001], and Crooker *et al.* [2003] have all observed specific cases where heat flux is correlated with pitch angle anisotropy. For a given F_H , heat flux is highest when the strahl is narrowest.

[7] Until recently, studies of electron heat flux and its correlations with solar wind parameters have not explicitly considered the contribution of pitch angle anisotropy [e.g., Feldman *et al.*, 1975, 1978; Scime *et al.*, 1994, 1999]. Meanwhile, studies addressing pitch angle anisotropy have tended to mention its relationship to electron heat flux only in passing, concentrating instead on potential electron scattering mechanisms or the magnetic field implications [e.g., Pilipp *et al.*, 1987a, 1987b; McComas *et al.*, 1989; Lin and Kahler, 1992; Fitzenreiter and Ogilvie, 1992; Ogilvie *et al.*, 1999; Chisham *et al.*, 2000; Zurbuchen *et al.*, 2001].

[8] This paper combines the two viewpoints, building on the approach introduced by Crooker *et al.* [2003]. By explicitly decomposing Q into its two components, anisotropy and number flux, we expose the fact that only anisotropy responds to local solar wind parameters, probably explaining why previous studies looking for consistent correlations with heat flux have been inconclusive. For instance, while heat flux has been observed to correlate with both magnetic field magnitude and anticorrelate with proton density, it does not do so consistently [Feldman *et al.*, 1976b]. To date, no heliospheric regulatory mechanisms

for electron heat flux have been found (e.g., see recent discussion by Scime *et al.* [2001]).

2. Data and Parameters

[9] This study uses Wind data from 1995 and 1996. We use 10 min averages of electron flux for energies between 10 eV and 1.3 keV from the 3DP instrument [Lin *et al.*, 1995]. Each time step consists of flux intensities from 13 pitch angle bins between 0° and 180° , aligned from parallel to antiparallel to the magnetic field, respectively. Electron heat flux values, calculated from the third moment of the total electron distribution at all energies as measured by 3DP, are also used. The Wind Solar Wind Experiment [Ogilvie *et al.*, 1995] and Magnetic Field Investigation [Lepping *et al.*, 1995] provide local plasma and field parameters.

[10] The data were sorted to exclude all times where Wind was inside the Earth's magnetosphere or within an interplanetary coronal mass ejection as identified by Cane and Richardson [2003] or the ISTP event catalog (<http://pwg.gsfc.nasa.gov/scripts/SWCatalog.shtml>) and where any of the instruments have significant data gaps (>10% of data missing over a 24 hour period). Efforts were also made to exclude intervals of counterstreaming electrons due to connection with the Earth's bow shock [Feldman *et al.*, 1975, 1982]. Typically, connection to the Earth's bow shock is assumed to occur when the angle between the local magnetic field direction and the spacecraft-Earth line is small ($0^\circ \leq \psi \leq 20^\circ$ and $160^\circ \leq \psi \leq 180^\circ$) [Gosling *et al.*, 1987; Skoug *et al.*, 2000]. Haggerty *et al.* [2000] showed that while most bow shock connections occur when θ is within 30° of the GSE X axis, sometimes less radial magnetic fields can still be connected. For the purposes of this study we use conservative bounds for ψ . Days where ψ fell within $0^\circ \leq \psi \leq 45^\circ$ and $135^\circ \leq \psi \leq 180^\circ$ for more than 10% of the time were removed. We note that we have not taken into account the effect of occasional thermal electron anisotropies that can extend to suprathermal energies and result in distributions that can mimic counterstreaming [c.f. Phillips *et al.*, 1989].

[11] To ensure that the remaining data intervals are long enough for meaningful correlation coefficients, we consider only time periods which are at least 3 days long. Time periods start and end at 0000 hours. This leaves 147 days in 1995 and 209 days in 1996 (times given in Tables 1 and 2), a total of 21,168 and 30,096 data points, respectively.

[12] From the pitch angle binned electron fluxes, the integrated flux over pitch angle at each time step, for each energy E , is

$$F_E = \sum_{i=1}^{13} j_i \sin \theta_i, \quad (1)$$

where j_i is the electron flux in each pitch angle bin, and θ_i is the pitch angle. This is related to the total number flux of suprathermal electrons by $\sum_E F_E = F_H$ for $E > 80$ eV. Since the number flux of electrons at each energy E drops off dramatically as E increases, it is helpful to use normalized flux for comparing pitch angle distributions of different energies. Following the normalization procedure used by

Table 1. Correlations of Observed $\log(Q)$ With F_{275} , A_E , and Q_M for 1995

Start day	End day	Cor(Q/F_{275})	Cor(Q/A)	Cor(Q/Q_M)
8	12	0.65	0.58	0.78
68	72	0.73	-0.03	0.85
73	82	0.79	0.45	0.96
86	94	0.55	0.75	0.94
97	101	0.57	0.03	0.54
106	113	0.63	0.77	0.89
116	128	0.75	-0.27	0.75
129	136	0.38	0.38	0.74
143	158	0.47	0.37	0.65
163	169	0.23	0.74	0.84
181	185	0.42	0.52	0.85
188	204	0.58	0.62	0.85
251	255	0.48	0.44	0.70
266	276	0.68	0.52	0.85
283	286	0.02	0.73	0.73
293	298	0.69	0.06	0.85
301	306	0.43	0.49	0.78
313	319	0.49	0.61	0.72
322	329	0.71	0.78	0.90
337	341	0.62	0.57	0.76
346	353	0.59	0.68	0.75
Mean		0.55	0.47	0.79

the Wind 3DP team for their routine pitch angle spectrogram displays [e.g., *Lin et al.*, 1995], we define the normalized pitch angle distributions at each time step and energy as

$$j_N = j_i / \langle j \rangle, \quad (2)$$

where $\langle j \rangle$ is the mean flux across all pitch angles. Figure 1 gives example pitch angle distributions at three different energies for a 10 min period of day 89 of 1995. There are two orders of magnitude difference between the unnormalized counts at the highest and lowest energies (Figure 1, top). The integral under each curve is the total number flux, F_E , at that energy for that time step (equation (1)). From the normalized counts defined in equation (2) (Figure 1, bottom), it is clear that in this case the shape of the pitch angle distribution is the same for all energies. Similar to *Crooker et al.* [2003], we use a variance parameter to quantify pitch angle anisotropy at each energy level:

$$A_E = \log(\text{Var}(j_N)) = \log\left(\frac{\sum_{i=1}^{13} (j_N - \langle j_N \rangle)^2}{\sum_{i=1}^{13} j_N}\right). \quad (3)$$

When $A_E \rightarrow -\infty$, the distribution is perfectly isotropic (corresponding to $\text{Var}(j_N) = 0$). In practice, A_E typically ranges from -3 to 1 , and the higher the value of A_E , the greater the anisotropy. Based only on 13 pitch angle bins, A_E is less noisy than other measures of anisotropy such as the skew of the pitch angle distribution or the width of its peak. Since we are using normalized flux values, j_N , A_E is dimensionless and independent of the total number of electrons and only parameterizes the shape of the distribution.

[13] As discussed in section 1, the amount of electron heat flux leaving the Sun, Q , should depend on both the total number flux of suprathermal electrons, F_H , and the shape of the electron pitch angle distributions, A_E . Figure 2 illustrates this relationship at one energy level in a day-long

interval of data from 1995. The top panel is the pitch angle spectrogram using normalized electron flux data at $E = 275$ eV. Blue represents the lowest counts and red represents the highest. The strahl appears as the red to yellow band primarily aligned with the magnetic field, indicating fields rooted at the Sun with away polarity. $\log(Q)$, in black, is plotted with A_E in the middle panel and $\log(F_E)$ in the bottom panel, both in red.

[14] Our anisotropy parameter, A_E , reflects the variation in strahl very well. It drops to its lowest values when the strahl essentially disappears at days 89.5–89.6 and after day 90.45. It is highest when the strahl intensity reaches red values, and it takes on intermediate values on days 90.1–90.3, when the strahl weakens preceding and during an excursion into the opposite polarity sector. It is also clear that heat flux, Q , responds sensitively to the changes in anisotropy from the middle panel. However, it is also apparent that heat flux exhibits an overall downward trend over this period in response to a steady decline in total suprathermal electron flux F_E (Figure 2, bottom). Thus Figure 2 illustrates that parameterizing the pitch angle anisotropy with A_E isolates the response of heat flux to the shape of the pitch angle distribution, effectively removing its dependence on integrated number flux, F_E .

3. Analysis

3.1. Correlations of Heat Flux and Anisotropy

[15] As discussed in section 1, heat flux should depend on F_H , the number flux of hot electrons in the solar wind. This can be expressed as $\sum_E F_E$, the sum of the total fluxes over all suprathermal energies. Hence we expect heat flux $\log(Q)$ to be correlated with any one value of $\log(F_E)$ as long as $E > 50$ – 100 eV. From section 2 and Figure 2, it is clear that at

Table 2. Correlations of Observed $\log(Q)$ With F_{275} , A_E , and Q_M for 1996

Start day	End day	Cor(Q/F_{275})	Cor(Q/A)	Cor(Q/Q_M)
7	10	0.55	0.85	0.91
20	26	0.71	0.53	0.82
31	34	0.35	0.74	0.81
38	48	0.56	0.61	0.83
49	55	0.57	0.67	0.81
57	61	0.51	0.67	0.72
62	74	0.65	0.53	0.87
75	82	0.60	0.60	0.81
83	86	0.66	0.66	0.83
91	95	0.45	0.72	0.83
98	103	0.68	0.63	0.91
117	128	0.62	0.85	0.86
139	142	0.89	0.89	0.97
143	148	0.72	0.84	0.90
151	176	0.83	0.73	0.94
177	183	0.67	0.59	0.87
185	220	0.69	0.72	0.88
222	231	0.70	0.65	0.89
235	238	0.57	0.30	0.78
239	243	0.49	0.53	0.70
244	255	0.63	0.66	0.87
290	294	0.54	0.64	0.79
299	305	0.75	0.30	0.80
308	318	0.55	0.79	0.88
328	333	0.76	0.20	0.84
349	358	0.61	0.42	0.76
Mean		0.63	0.63	0.84

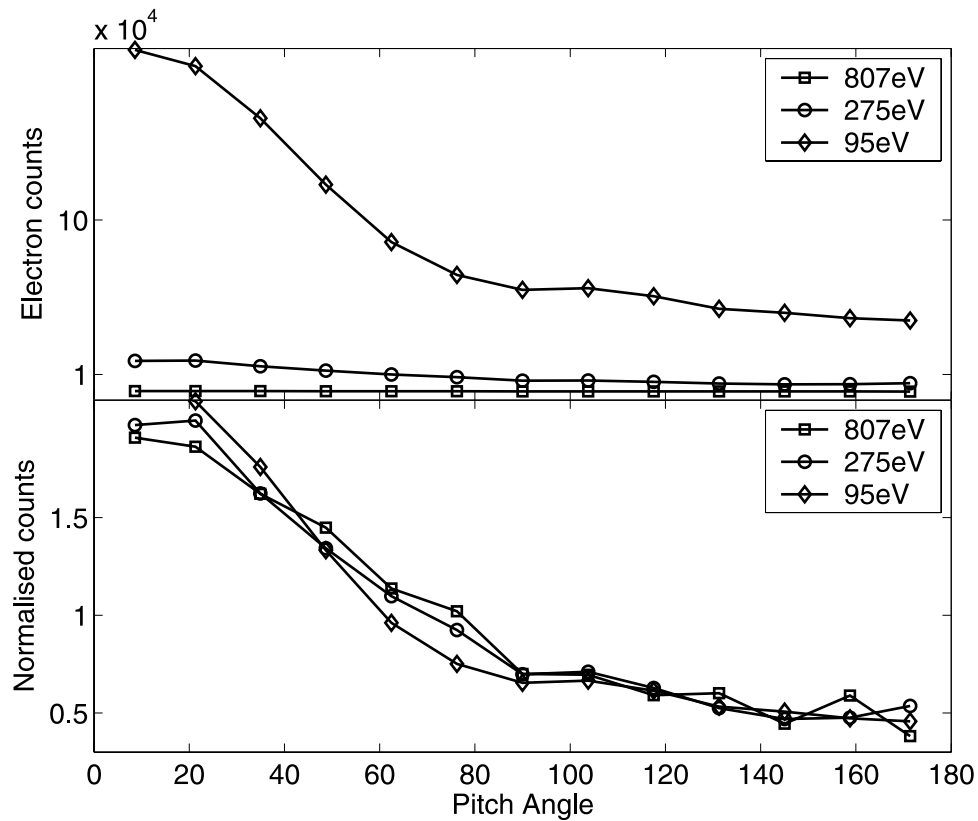


Figure 1. (top) Unnormalized and (bottom) normalized pitch angle distributions at different suprathermal energies for day 89, 1995.

times, heat flux follows both F_E and the pitch angle anisotropy A_E . Figures 3a and 3b show that these relationships hold throughout the solar wind. These are two-dimensional (2-D) histograms of $\log(Q)$ with $\log(F_E)$ and

anisotropy A_E , respectively, at 275 eV. The points are all the data within the times given in Tables 1 and 2. The color scale gives the number of data points in each 2-D box. Positive correlations between $\log(Q)$ and both $\log(F_E)$ and

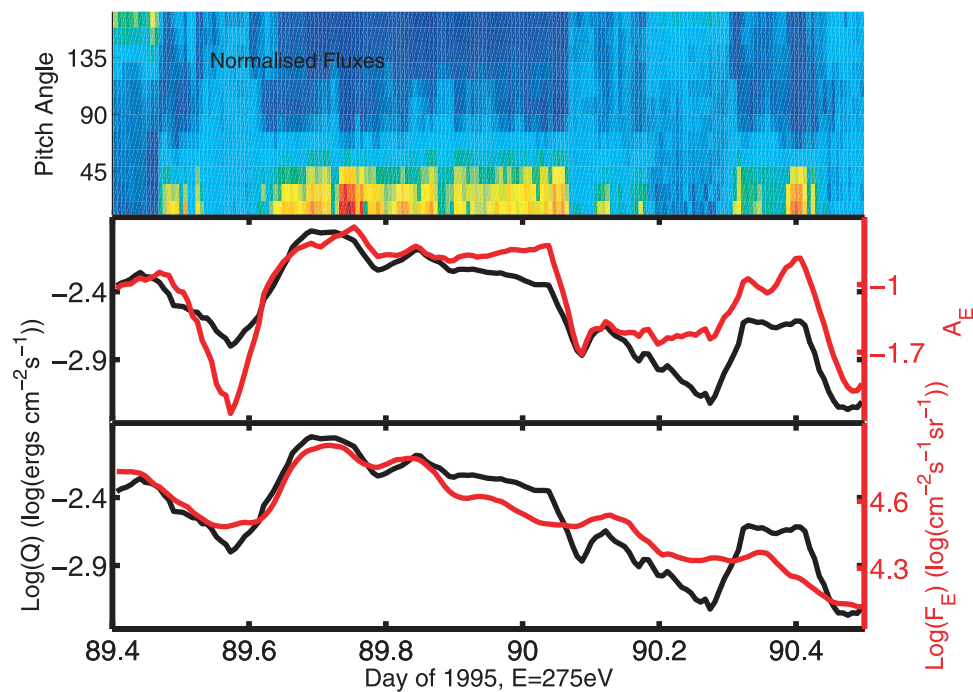


Figure 2. (top) Normalized pitch angle spectrogram, and corresponding values of heat flux, Q , anisotropy, A_E , and log number flux, $\log(F_E)$, for electrons at $E = 275$ eV.

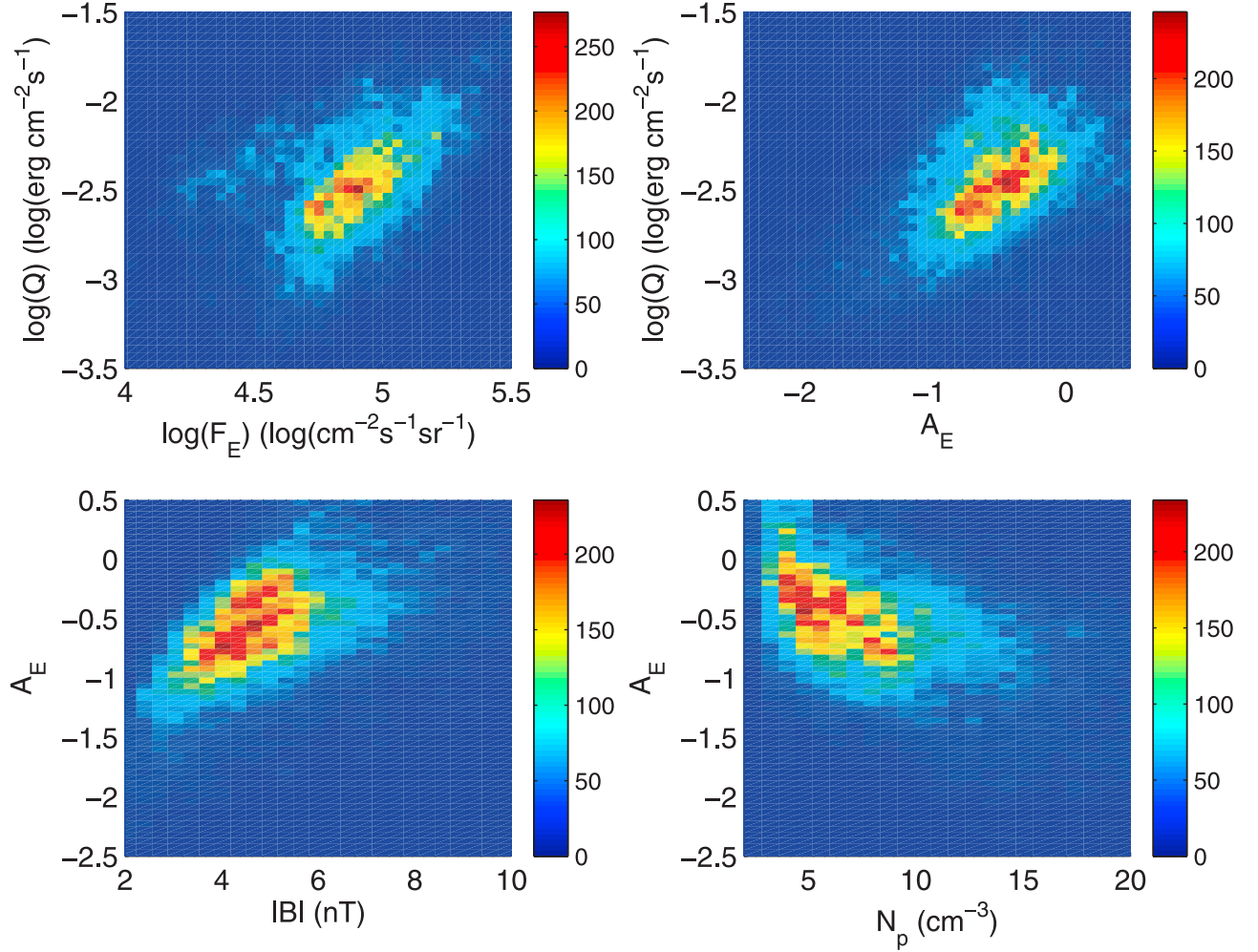


Figure 3. Two-dimensional (2-D) histograms of heat flux correlations and anisotropy correlations. (a) The log heat flux and log total flux at $E = 275$ eV, (b) log heat flux and anisotropy, A_E . A positive correlation is evident for both. (c) The 2-D histogram of A_E and magnetic field strength, $|\mathbf{B}|$, (d) A_E and density N_p .

A_E are evident, with linear correlation coefficients of 0.62 and 0.54, respectively. Figure 4 shows how the correlation coefficients between $\log(Q)$ and $\log(F_E)$ depend upon energy, E . The dotted vertical line at $E = 80$ eV marks the boundary between core and suprathermal electrons. The plot makes clear that suprathermal electrons carry the heat flux and that the correlations between $\log(F_E)$ and $\log(Q)$ are good for the whole of the suprathermal range, 80–1300 eV.

[16] As discussed in section 1, pitch angle anisotropy has been shown to correlate with in situ solar wind parameters at certain times in the solar wind, particularly plasma density, N_p , and local plasma beta, β , proportional to $N_p/|\mathbf{B}|^2$, where $|\mathbf{B}|$ is the magnetic field strength. Pitch angle isotropizations at sector boundaries have also been noted. Figure 5 shows 2 days of data where correlations of A_E with $|\mathbf{B}|$ and N_p (correlation coefficients are 0.66 and -0.50 , respectively) are evident in the vicinity of the multiple sector boundaries, apparent in Figure 2. A_E is plotted in a negative sense in the upper panel since it anticorrelates with N_p . As above for heat flux, these

relationships continue to hold throughout the solar wind. Figures 3c and 3d show the 2-D histograms for our anisotropy parameter, A_E , with $|\mathbf{B}|$ and N_p , respectively. Correlations between A_E and $|\mathbf{B}|$ and N_p are evident with linear correlation coefficients of 0.47 and -0.44 , respectively. Anisotropy increases with magnetic field intensity and decreases with increasing plasma density. The anticorrelation with N_p is consistent with previous observations by *Pilipp et al.* [1990] and *Ogilvie et al.* [1999, 2000]. From Figure 6 it is clear that there is no correlation between A_E and $\log(F_E)$ (correlation coefficient over 1995 and 1996 is -0.04), confirming their expected independence.

3.2. Multiple Linear Regression Models for Heat Flux and Anisotropy

[17] Section 3.1 examined the relationships between Q , F_E , and A_E . Equation (4) quantifies these relationships by decomposing Q into the two (independent) parameters. Further, equation (5) quantifies the demonstrated relationships between the shape of the pitch angle distribution, A_E ,

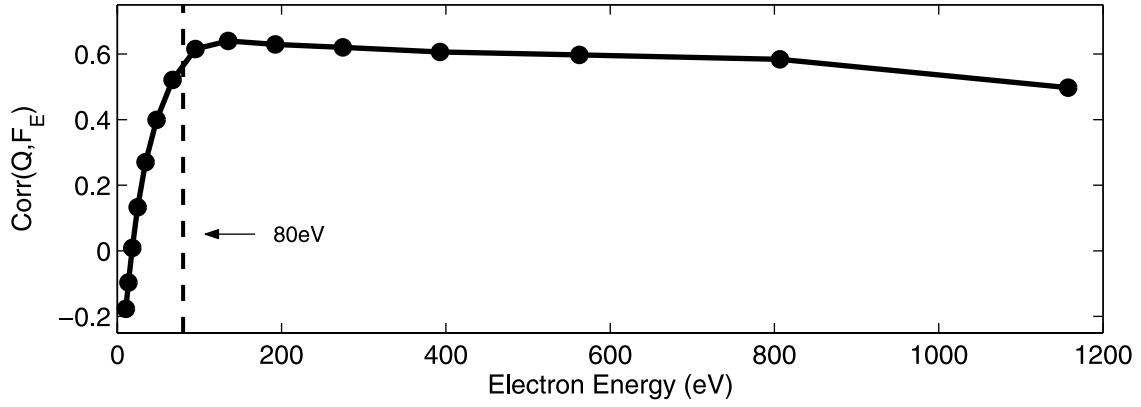


Figure 4. Variation of the correlation coefficients between $\log(Q)$ and $\log(F_E)$ with electron energy E . Correlation coefficients are calculated for 1995 and 1996 using data from the times give in Tables 1 and 2.

and the magnetic field intensity $|\mathbf{B}|$ and solar wind density N_p .

$$\log(Q_M) = f \log(F_E) + aA_E + c \quad (4)$$

$$A_M = b|\mathbf{B}| + nN_p + d \quad (5)$$

In these equations, the “M” subscript stands for “model,” and f , a , c , b , n , and d are constants. Equation (5) may not be an optimal parameterization for A_E as A_E may depend on other solar wind parameters, notably proton temperature [c.f. *Crooker et al.*, 2003], or a nonlinear dependence like $N_p^{1/2}$ might be better. However, we note that our anisotropy model performs better than a regression on parameters such as plasma beta or $|\mathbf{B}|^2$.

[18] To obtain the best fit coefficients f , a , c , b , n , and d , the models are fit by multiple linear regression to 1996 data. Fitting to just 1 year allows for a consistency check, since if the models are viable then the best-fit coefficients calculated using 1 year of data should also apply to the other year. Using electrons at 275 eV as a representative suprathermal population, we get the following parameterization:

$$\log(Q_M) = 0.79 \log(F_E) + 0.32A_E - 6.26 \quad (6)$$

$$A_M = 0.16|\mathbf{B}| - 0.05N_p - 1.00. \quad (7)$$

To validate these coefficients, $\log(Q_M)$ and A_M are then computed using observed $\log(F_E)$, A_E , $|\mathbf{B}|$, and N_p for both 1995 and 1996 and compared with the observed $\log(Q)$ and

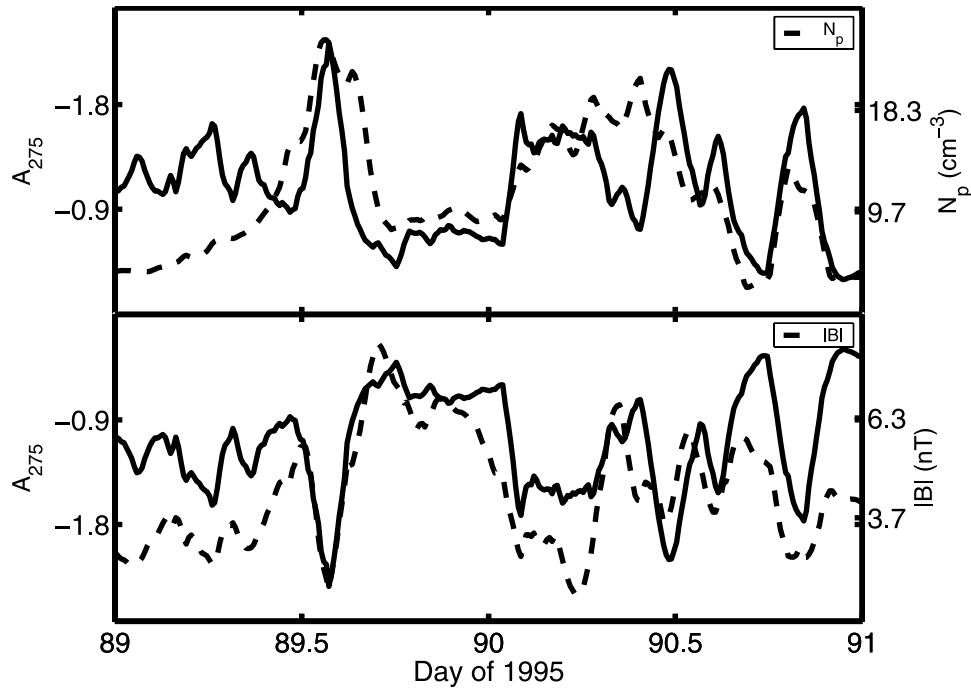


Figure 5. Variation of A_E with N_p and $|\mathbf{B}|$, for $E = 275$ eV. Correlations of A_E with N_p and $|\mathbf{B}|$ for this time period are -0.50 and 0.66 , respectively.

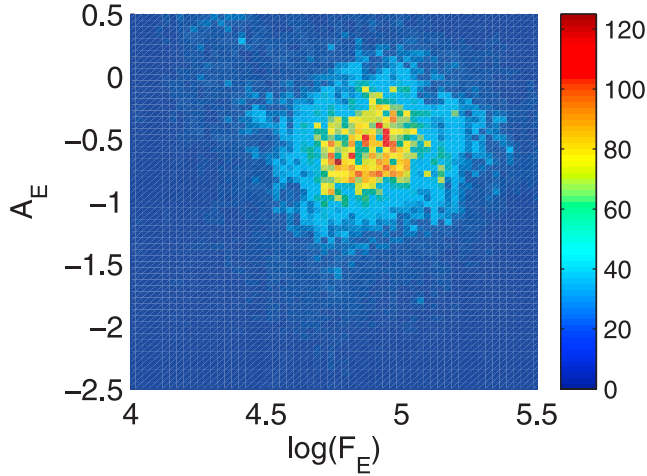


Figure 6. The 2-D histogram of log number flux and anisotropy at $E = 275$ eV.

A_E . Examples of $\log(Q_M)$ and A_M for $E = 275$ eV and their fit to Q and A_E are shown in Figures 7 and 8, respectively. In each figure, the blue line representing the models reproduces the observed data remarkably well.

[19] Tables 1 and 2 list the linear correlation coefficients for Q with F_E , A_E , and Q_M . Tables 3 and 4 list the coefficients for A_E with $|\mathbf{B}|$, N_p , and A_M for each time period in 1995 and 1996. The decomposition of heat flux into F_E and A_E works extremely well throughout both years, with a high overall correlation of 0.82 between Q_M and Q . The model for A_E fits more variably over the whole of 1995

and 1996, with the mean correlation between A_M and A_E being 0.64. Considering the potential complexity of the interplay of various pitch angle scattering mechanisms, the fits perform well and provide support for the hypothesis that A_E is mainly regulated by in situ solar wind. In nearly all time periods for both years, $\log(Q_M)$ and A_M correlate better with $\log(Q)$ and A_E , respectively, than either of the dependent parameters, as reflected by the means at the bottom of each table.

[20] Using 95% confidence intervals to find the upper and lower bounds of the models results in a mean confidence interval range of 0.16 for Q_M and 0.06 for A_M , both less than half a sigma of the total distribution. Using either upper or lower limits of the fitted parameters to calculate Q_M or A_M does not affect the calculated correlation coefficients between the models and data.

[21] The relative importance of the independent variables on the heat flux and anisotropy can now be investigated using the models. This cannot be done, however, by comparing the model coefficients in equations (6) and (7) because the means and scales of the independent variables, $\log(F_E)$ and A_E , $|\mathbf{B}|$ and N_p are not the same. To analyze respective dominance, these variables need to be normalized, using the standard formula

$$X_N = \frac{X - \langle X \rangle}{std(X)}, \quad (8)$$

where $\langle X \rangle$ is the mean of the time series X , and $std(X)$ is its standard deviation. Normalization results in a new set of variables, Q_N , F_{NE} , A_{NE} , $|\mathbf{B}|_N$, and N_{Np} , all with mean zero and standard deviation one. Fitting the models to these

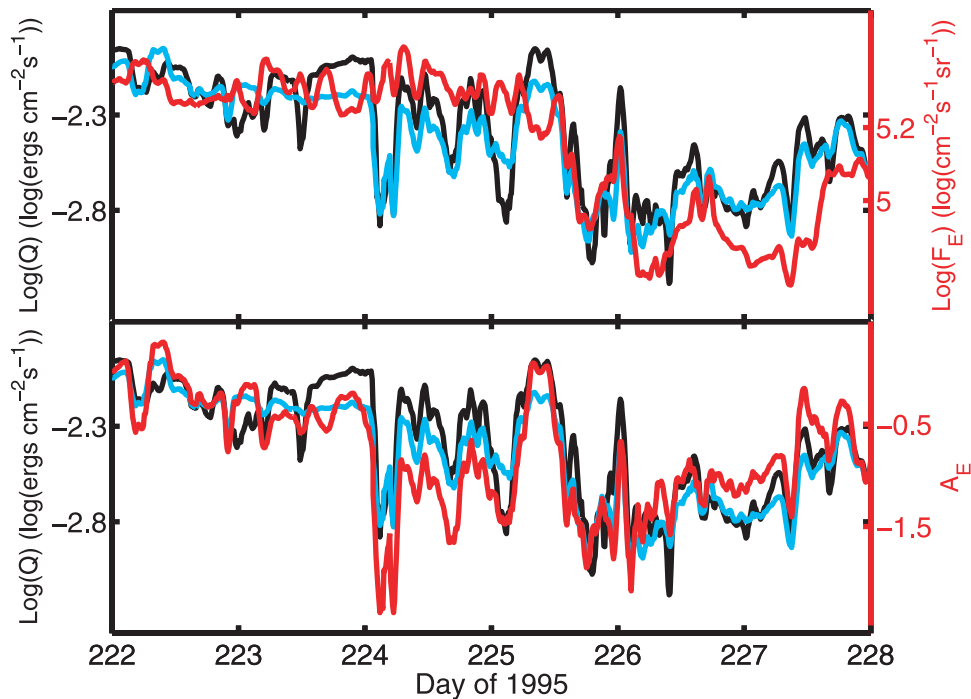


Figure 7. The $\log(Q_M)$ for electrons at 275 eV and days 222–228 of 1996. The correlation coefficient between $\log(Q_M)$ (in blue) and $\log(Q)$ (in black) is 0.92.

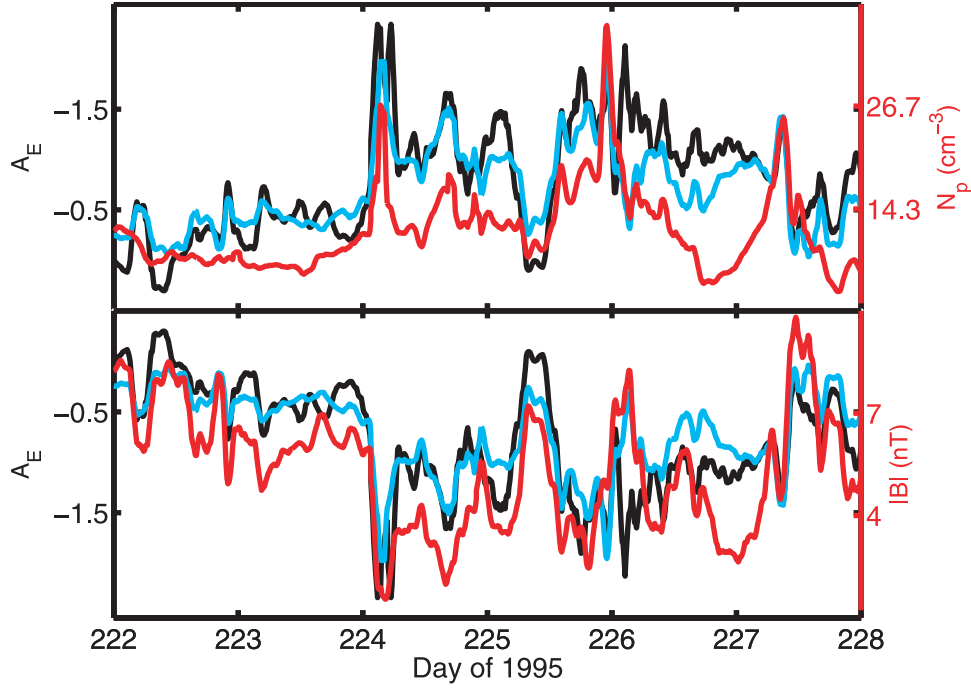


Figure 8. A_M for electrons at 275 eV and days 222–228 of 1996. The correlation coefficient between A_M (in blue) and A_E (in black) is 0.85.

variables at $E = 275$ eV and applying multiple linear regression in the same manner as above, yields

$$\log(Q_{NM}) = 0.57 \log(F_{NE}) + 0.54 A_{NE} \quad (9)$$

$$A_{NM} = 0.59 |B|_N - 0.47 N_{Np}. \quad (10)$$

These fitted coefficients now reflect the relative contributions of the variables. Equation (9) shows that total suprathermal electron flux and pitch angle anisotropy control

variability in heat flux almost equally. Equation (10) shows that the magnetic field slightly dominates the plasma density in the control of pitch angle anisotropy. While the respective weights of magnetic field and density on anisotropy should be treated with circumspection, the nearly equal influences of total electron number flux and pitch angle anisotropy are significant due to the excellent fit

Table 3. Correlations of Observed A_E With $|B|$, N_p , and A_M for 1995

Start doy	End doy	Cor($A/ B $)	Cor(A/N_p)	Cor(A/A_M)
8	12	0.47	-0.03	0.64
68	72	0.25	-0.63	0.56
73	82	0.59	-0.62	0.78
86	94	0.82	-0.39	0.89
97	101	-0.31	-0.68	0.45
106	113	0.60	0.08	0.60
116	128	0.	-0.49	0.37
129	136	0.29	-0.10	0.25
143	158	0.37	-0.60	0.75
163	169	0.40	-0.26	0.61
181	185	0.52	-0.75	0.74
188	204	0.43	-0.47	0.74
251	255	0.52	-0.12	0.74
266	276	0.21	-0.24	0.40
283	286	0.52	-0.49	0.67
293	298	-0.22	-0.49	0.04
301	306	0.27	-0.47	0.56
313	319	0.37	-0.35	0.53
322	329	0.55	-0.45	0.69
337	341	0.56	-0.12	0.67
346	353	0.45	-0.48	0.63
Mean		0.36	-0.39	0.59

Table 4. Correlations of Observed A_E With $|B|$, N_p , and A_M for 1996

Start doy	End doy	Cor($A/ B $)	Cor(A/N_p)	Cor(A/A_M)
7	10	0.76	-0.59	0.82
20	26	0.50	-0.32	0.54
31	34	0.63	0.11	0.69
38	48	0.33	-0.48	0.69
49	55	0.13	-0.50	0.57
57	61	0.60	-0.29	0.71
62	74	0.23	-0.45	0.51
75	82	0.52	-0.26	0.66
83	86	0.64	-0.10	0.77
91	95	0.71	-0.33	0.66
98	103	0.55	0.21	0.31
117	128	0.77	-0.54	0.83
139	142	0.79	-0.50	0.92
143	148	0.62	-0.71	0.83
151	176	0.50	-0.23	0.60
177	183	0.50	-0.40	0.68
185	220	0.58	-0.27	0.69
222	231	0.67	-0.61	0.83
235	238	0.03	-0.27	0.36
239	243	0.44	-0.12	0.69
244	255	0.55	-0.04	0.66
290	294	0.48	-0.80	0.84
299	305	0.41	-0.44	0.72
308	318	0.56	-0.18	0.59
328	333	0.51	-0.68	0.80
349	358	0.74	-0.51	0.86
Mean		0.53	-0.36	0.69

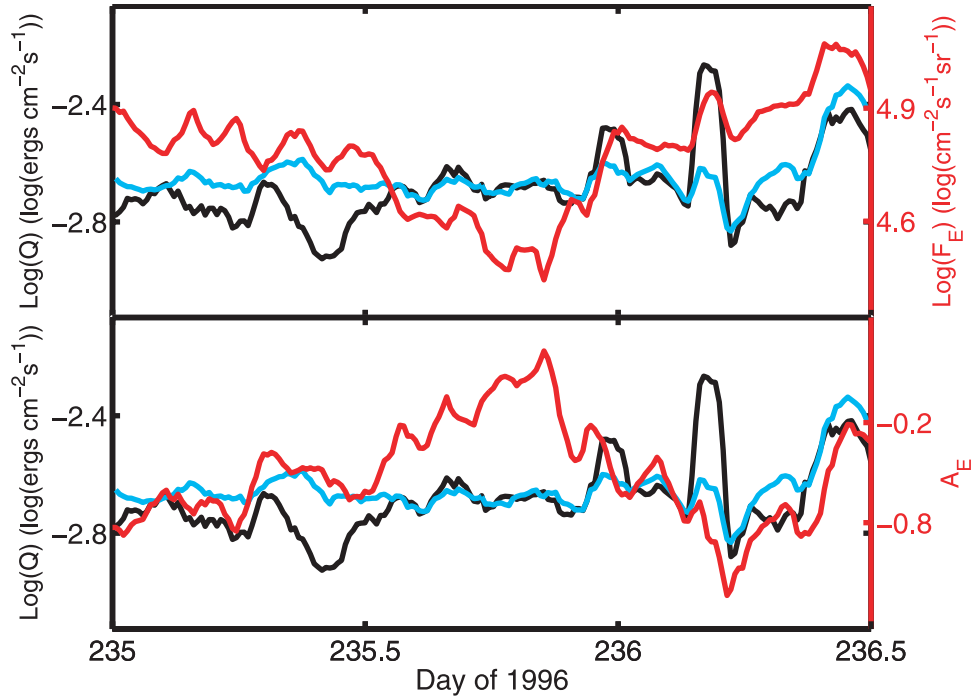


Figure 9. Example of opposite changes in (top) $\log(F_E)$ and (bottom) A_E giving no overall change in $\log(Q)$ (in black). The model Q_M (in blue) deals with this very well.

of Q_M . This key result helps explain why correlative studies that treat heat flux as a single variable yield inconclusive results.

[22] Variations in the total suprathermal number flux are likely due to variability in the solar source regions, for example magnetic field line footpoint motions and exchanges on the Sun [Fisk et al., 1999; Gosling et al., 2004] and/or strong Coulomb scattering very near the Sun (J. T. Gosling, private communication, 2004). It is unlikely that F_E is affected by in situ processes at 1 AU as it is not correlated with solar wind parameters. However, variations in A_E are likely to arise from in situ processes. Figure 9 demonstrates the need for incorporating both parameters, F_E and A_E , into one equation. It gives an example of when a rise in one offsets a drop in the other with no net observed change in $\log(Q)$ during 2 days of 1996. Toward the end of day 235, $\log(F_E)$ drops and A_E rises while the heat flux $\log(Q)$ remains steady. The model, Q_M , mirrors the heat flux response almost exactly.

[23] Anisotropy in turn responds to changes in $|\mathbf{B}|$ and N_p . At times, as is evident from Tables 3 and 4, A_E is much better correlated with $|\mathbf{B}|$ than with N_p and vice versa. At others it is equally well correlated with both. This inconsistency suggests that there might be more than one scattering process active in the solar wind. The correlation of A_E with both $|\mathbf{B}|$ and N_p suggests physical processes perhaps limited by plasma beta or Alfvén speed. The question of multiple scattering processes is addressed further later in this paper.

[24] The models, Q_M and A_M , can explain many of the previously reported results. At sector boundaries, where typically $|\mathbf{B}|$ is low and N_p is high, anisotropy will be low (from equation (7)), i.e., pitch angle isotropization is expected in these regions. If there is a significant drop

in A_E , a responding drop in Q is also expected (from equation (6)). Often at sector boundaries, a drop in F_E is observed coincident with a drop in A_E [McComas et al., 1989] (J. T. Gosling, private communication, 2004), and in these cases a significant heat flux drop is expected. Similarly, we would predict heat flux drops and pitch angle isotropization at any region of very low $|\mathbf{B}|$ or high-beta plasma solar wind. These effects are exactly what has been observed [Pilipp et al., 1990; McComas et al., 1989; Ogilvie et al., 1999; Chisham et al., 2000; Zurbuchen et al., 2001; Crooker et al., 2003]. Away from sector boundaries, where $|\mathbf{B}|$ is higher and N_p lower, A_M should be higher, i.e., there will be a stronger strahl. Again this is what is observed [Pilipp et al., 1990; Scime et al., 1994; Ogilvie et al., 1999, 2000].

3.3. Stream Structure

[25] There has been some difference reported in suprathermal pitch angle distributions between fast and slow solar wind. As mentioned above, the strahl is much narrower, i.e., the electron pitch angle distributions are more anisotropic, in fast wind compared with slow wind [Feldman et al., 1978; Pilipp et al., 1990; Scime et al., 1999, 2001; Ogilvie et al., 1999]. There is some evidence for the pitch angle distributions in fast wind to be more anisotropic at higher energies [Feldman et al., 1978; Pilipp et al., 1987a; Ogilvie et al., 2000], although this has not been consistently observed [Hammond et al., 1996]. The pitch angle distribution of the strahl in fast wind, however, broadens faster for lower-energy electrons than for the higher-energy electrons [Hammond et al., 1996], implying that the scattering process might be energy-dependent. There does not seem to be an energy dependence in pitch angle anisotropy near sector boundaries or in slow wind [Pilipp et al., 1987a].

Table 5. Mean Parameter Values in Fast and Slow Wind Across 1995 and 1996

Parameters	Slow Wind	Fast Wind
$\log(Q)$	-2.49	-2.46
A_E	-0.81	-0.08
$\log(F_E)$	4.88	4.72
$ \mathbf{B} $	4.68	5.33
N_p	11	4

[26] For the days given in Tables 1 and 2, periods of fast and slow wind were separated. Fast wind was selected where $|\mathbf{V}| \geq 520$ km/s, $N_p \leq 6$ cm⁻³, and $T_p \geq 8 \times 10^4$ K. Stream interaction regions were removed, and a minimum of 2 days of continuous data were required. Remaining are 85 and 133.5 days of slow wind data from 1995 and 1996, respectively, and only 14 and 8.5 days, respectively, of fast wind data. Table 5 gives mean values of the parameters in fast and slow wind for $E = 275$ eV. The values of $\log(Q)$ and A_E are consistent with reported trends. Heat flux is the same in fast and slow wind, as *Scime et al.* [1999, 2001] found using 10 years of Ulysses data. A_E , however, is much higher in fast wind than in slow wind, consistent with previous studies reporting that pitch angle distributions are more anisotropic in fast solar wind streams.

[27] The values of $\log(F_E)$, $|\mathbf{B}|$, and N_p listed in Table 5 reflect the complicated interplay between these parameters. $|\mathbf{B}|$ is slightly higher in fast wind, which could contribute to the higher anisotropy, but the most significant difference between regimes is the value of N_p . Plasma density is much lower in fast wind, which presumably reduces suprathermal electron scattering, leading to a higher value of A_E (since anisotropy and density are anticorrelated). Given the much higher value of A_E there and the finding in section 3.2 that $\log(Q)$ is equally correlated with both $\log(F_E)$ and A_E , it is surprising to find that $\log(Q)$ is not higher in fast wind, since F_E is not significantly lower to counteract the increase in A_E . Since most of our data are from slow wind (and some stream interaction regions), the model coefficients found in section 3.2 reflect primarily slow wind characteristics. If the balance between F_E and A_E were different in fast wind, with F_E more dominant, then the relative values of $\log(Q)$, $\log(F_E)$, and A_E across the different types of solar wind could be explained. To test for this possibility, we repeat the analysis in section 3.2 separately for the two solar wind regimes.

[28] To perform multiple linear regression for the different regimes, we fit Q_M to 1995 fast wind data, since there are more data for fast streams in 1995 than in 1996. For consistency we also fit Q_M to 1995 slow wind data. Table 6 gives the resulting model coefficients for both unnormalized and normalized variables, where the latter can be compared for the relative importance of the parameters, and Table 7 gives the mean correlation coefficients over both 1995 and 1996.

[29] The values in Table 6 indicate that in slow wind both total electron number flux and pitch angle anisotropy remain equally important in determining the value of the electron heat flux. The fits of Q_M in slow wind are extremely good (overall correlation of 0.86), providing excellent support for the phenomenological picture of slow wind electron heat flux being a product of both the number of suprathermal electrons present and how narrowly they

stream along the interplanetary magnetic field. In contrast, in fast wind, total suprathermal electron number flux, F_E , is about twice as dominant as pitch angle anisotropy, A_E , in determining electron heat flux. Hence the small reduction in F_E in fast wind could be enough to counteract the increase in A_E and explain the lack of response of $\log(Q)$ to A_E there, as anticipated.

[30] Table 7 indicates that Q_M does not provide a good fit in fast wind, implying that there exist factors that we have failed to account for, which are not important in slow wind (where the fits are uniformly excellent). Of the eight fast wind time periods over 1995 and 1996, two have very poor fits of Q_M to Q (correlation coefficient ~ 0.15), and these considerably lower the resultant mean correlation, which would be 0.60 without them. Nevertheless, Q_M certainly does not seem to capture the behavior of the Q in the fast wind as well as it does in slow wind. While this could be due to the lack of parameter variability in fast wind, the fact that the fits of A_M remain good in fast wind argues against this explanation.

[31] For A_M , the model coefficients also vary between fast and slow wind. In fast wind, the higher model coefficients for $|\mathbf{B}|$ and N_p are expected given the uniformly higher anisotropy in fast wind. The relative weights of the coefficients (for the normalized model A_{NM}) are given by their ratio $b/|n|$. For slow wind, $b/|n| = 1.61$ and in fast wind $b/|n| = 1.26$. Hence the magnetic field dominates density in determining pitch angle distributions more in slow than in fast wind. While Q_M and A_M correlation coefficients over all solar wind are similar to values for slow wind because slow wind dominates both 1995 and 1996, for the normalized A_{NM} model, $b/|n|$ matches the fast wind ratio (1.26) rather than the slow (1.61). This may be due to the influence of stream interaction regions, which were excluded from the stream-sorted data. There N_p is high and possibly instrumental in scattering the suprathermal electrons.

[32] In summary, fitting the models to fast and slow wind at $E = 275$ eV suggests that (1) in correlations with electron heat flux, the number flux of hot electrons is roughly twice as dominant as pitch angle anisotropy in fast wind, while they have almost equal influence in slow wind; (2) our model Q_M may not account for an additional influence on heat flux in fast wind, which is not significant in slow wind, where the model fits excellently; (3) in correlations with

Table 6. Model Coefficient Values for Fast and Slow Wind as Fitted to 1996 Data for $E = 275$ eV^a

Stream	Model	a_i	b_i	c_i
All solar wind	Q_M	0.79	0.32	-6.26
Fast wind	Q_M	0.58	0.15	-5.04
Slow wind	Q_M	0.73	0.42	-5.58
Norm all solar wind	Q_{NM}	0.57	0.54	-
Norm fast wind	Q_{NM}	0.62	0.33	-
Norm slow wind	Q_{NM}	0.59	0.58	-
All solar wind	A_M	0.16	-0.05	-1.00
Fast wind	A_M	0.24	-0.27	-0.32
Slow wind	A_M	0.12	-0.03	-1.14
Norm all solar wind	A_{NM}	0.59	-0.47	-
Norm fast wind	A_{NM}	0.71	-0.57	-
Norm slow wind	A_{NM}	0.48	-0.30	-

^aHere a_i , b_i , c_i correspond to the two models: $\log(Q_M) = f \log(F_E) + aA + c$ and $A_M = b|\mathbf{B}| + nN_p + d$ and their normalized versions.

Table 7. Mean Model Correlation Coefficients for Fast and Slow Wind for 1995 and 1996

Stream	Corr(Q/Q_M)	Corr(A/A_M)
All solar wind	0.82	0.64
Fast wind	0.45	0.63
Slow wind	0.86	0.64

pitch angle anisotropy, the magnetic field is more influential in slow than fast wind.

3.4. Energy Dependencies

[33] The analysis detailed in sections 3.2 and 3.3 is confined to electrons at $E = 275$ eV but can be performed for all energies in the suprathermal range to test for energy dependence. Because some energy dependence has been reported in pitch angle anisotropy for fast wind, while none has been found in slow wind [Feldman *et al.*, 1978; Pilipp *et al.*, 1987a; Ogilvie *et al.*, 1999, 2000], we apply the analysis separately to fast and slow wind for energies in the range 80–830 eV.

[34] Figure 10 shows the variation of A_E with energy for fast and slow wind. The greater pitch angle anisotropy in fast wind is evident for all energies. There is little variation of A_E with energy in slow wind for $E < 400$ eV with a slight increase at the higher energies, consistent with the trends found by Feldman *et al.* [1978] and Pilipp *et al.* [1987a]. In fast wind, however, the anisotropy drops off slowly with increasing energy. If a change in anisotropy with energy corresponds to a change in the scattering rate of electrons at that energy, then the positive and negative gradients at higher energies for slow and fast wind, respectively, could be a result of different scattering mechanisms.

[35] Feldman *et al.* [1978], Pilipp *et al.* [1987a], and Ogilvie *et al.* [2000] all found an increasing pitch angle anisotropy with energy in fast wind (opposite to the trend in Figure 10), while Hammond *et al.* [1996] found no consistent energy dependence in fast wind. Since Feldman *et al.* [1978] analyzed energies limited to 60–300 eV, our results are consistent, since from 60 eV the anisotropy does increase (not shown). However, both Pilipp *et al.* [1987a] and Ogilvie *et al.* [2000] analyze energies up to 800–1000 eV (within our range). Although they both use (differ-

ent) measures of strahl angular width to parameterize pitch angle anisotropy different from our A_E , the opposite results we obtain do not appear to be a factor of different parameterization. While the examples of pitch angle distributions at each energy given by Pilipp *et al.* [1987a] show a clear increase in anisotropy with energy before any parameterization is performed, our pitch angle distributions show the opposite, more isotropic distributions at higher energies. Although Pilipp *et al.* [1987a] analyzed Helios data at 0.3 AU, a different heliocentric distance cannot explain the results of Ogilvie *et al.* [2000] since they used Wind data at 1 AU. These inconsistencies need further investigation.

[36] The correlation coefficients of anisotropy A_E with solar wind parameters also vary with energy as shown in Figure 11 for slow and fast solar wind. The regression fit error bars on the fitted model coefficients are negligible and hence not shown. The absolute correlation coefficients of A_E with N_p are plotted to account for their anticorrelation. In both regimes it is clear that $|\mathbf{B}|$ correlates better with A_E for all energies. For $E < 300$ eV, however, the correlation coefficients of A_E with $|\mathbf{B}|$ drop and those with N_p rise. This suggests that for the lowest suprathermal energies, local solar wind plasma density might be more influential in determining the pitch angle anisotropy in both fast and slow wind.

[37] This possibility can be further investigated by analyzing the normalized coefficients with energy (from model 10) for each energy. Figure 12 gives the coefficients, b and n , for A_{NM} in fast and slow wind for $|\mathbf{B}|$ and N_p , respectively. In both solar wind regimes the density becomes more influential (on a par with $|\mathbf{B}|$) at the lower suprathermal energies ($E < 200$ eV), mirroring the correlations seen in Figure 11. However, while the density coefficient in slow wind is quite steady at the higher energies, in fast wind it drops significantly. This implies two things: first, that the scattering mechanisms active in fast wind are energy dependent at the highest energies, and second, that different scattering mechanisms are present in fast and slow solar wind. Energy-dependent scattering might imply a Coulomb process, but this seems inconsistent with the much lower particle densities in fast solar wind (see discussion by Ogilvie *et al.* [2000]). Wave-particle interactions could also be responsible. Ion acoustic scattering and whistler and

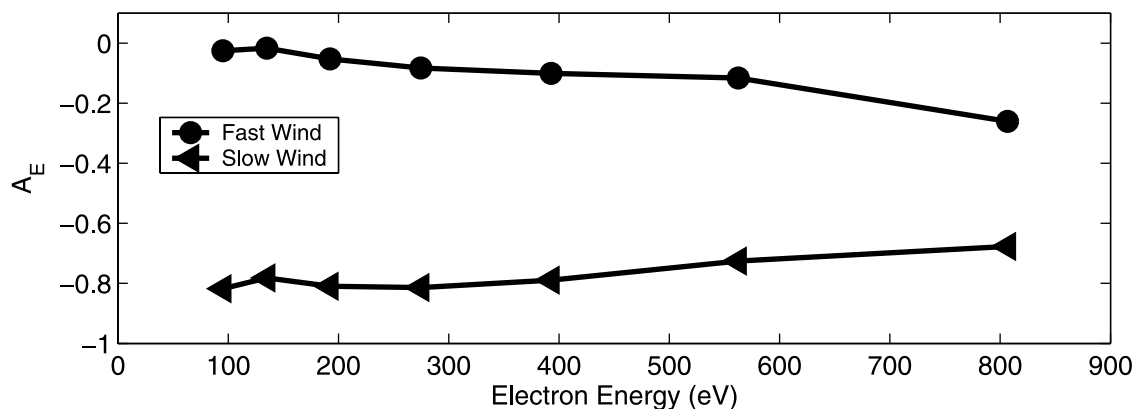


Figure 10. Variation of A_E with suprathermal energy, E , for fast and slow wind. Data covers both 1995 and 1996. Both slow and fast wind show steady A_E for energies below ~ 300 eV, with A_E then increasing for higher energies in slow wind, and decreasing in fast wind.

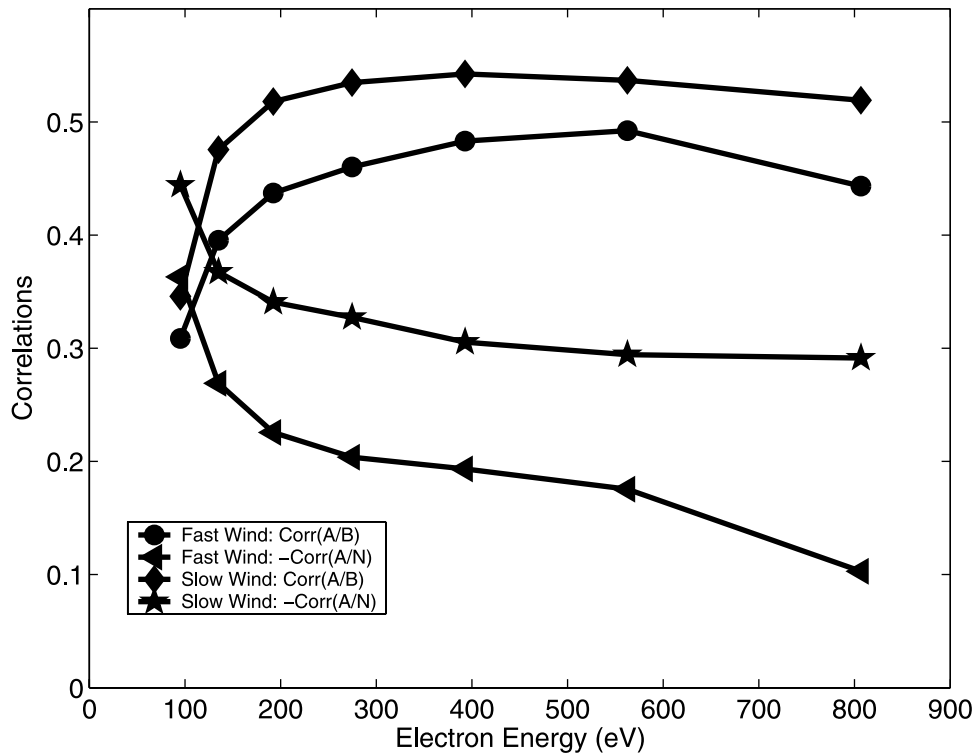


Figure 11. The correlation coefficients between A_E and solar wind parameters plotted against energy.

Alfvén wave instabilities have been previously discounted as mechanisms [Pilipp *et al.*, 1987b; McComas *et al.*, 1989; Scime *et al.*, 1994, 1999, 2001], but these studies relied on correlations with electron heat flux. Fresh analysis, consid-

ering only pitch angle anisotropy, might show that these mechanisms do have a role to play in determining heat flux. Additional studies of the energy-dependence and parameter-dependence of scattering in individual events in the different

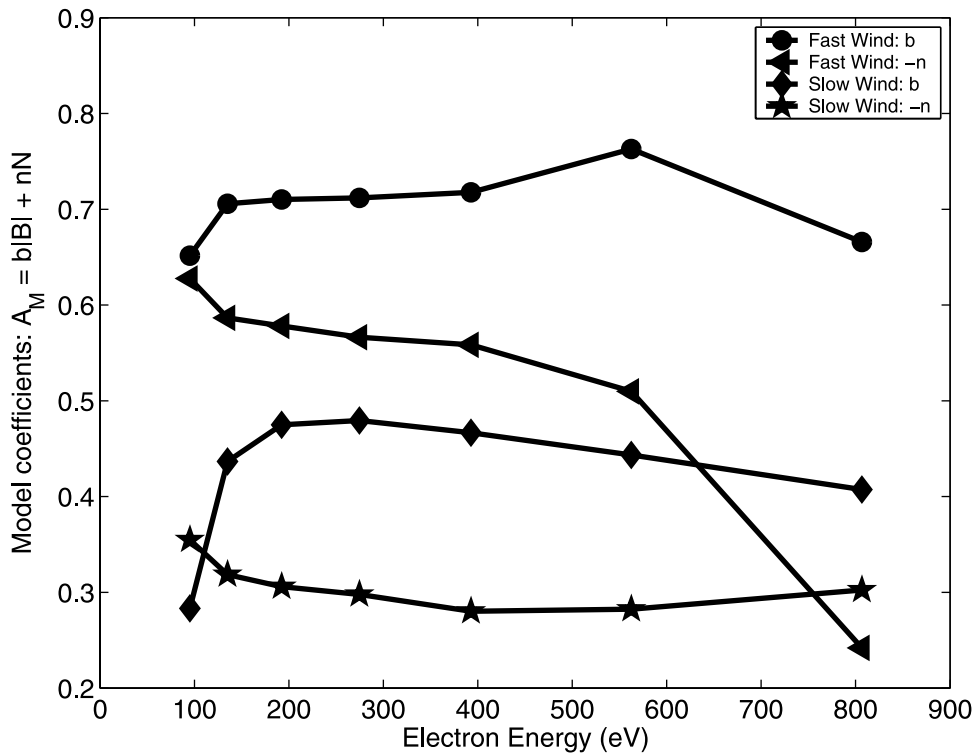


Figure 12. Variation of fitted model coefficients for A_M with energy.

solar wind regimes are required to further constrain potential scattering processes.

4. Discussion and Conclusions

[38] The phenomenological model of electron heat flux proposed by *Feldman et al.* [1975] and *Scime et al.* [1994] has been quantified and analyzed for dependence on solar wind parameters. Their model assumes that electron heat flux is a function of both the total number of suprathermal electrons, F_E , and their relative drift to the total electron population $|\Delta\mathbf{V}_H|$. If $|\mathbf{Q}| \sim |\Delta\mathbf{V}_H|F_H$, then $\log(Q) \sim \log(|\Delta\mathbf{V}_H|) + \log(F_H)$. We make explicit the connection between $\log(|\Delta\mathbf{V}_H|)$ and pitch angle anisotropy, parameterized by A_E , leading directly to the model Q_M . Pitch angle anisotropy, A_E , in turn correlates with magnetic field strength $|\mathbf{B}|$ and anticorrelates with plasma density N_p .

[39] The models of heat flux, Q_M , and pitch angle anisotropy, A_M , fitted 2 years of data very well. The models reproduce reported observations and patterns including heat flux dropouts and pitch angle isotropization in high-beta plasma regions like sector boundaries. Heat flux drops will be most noticeable in regions where both anisotropy and number flux drop together. Such events could be due to magnetic field line disconnection events from the Sun. Heat flux dropouts where only anisotropy is low and number flux remains constant are probably due to pitch angle scattering.

[40] In line with previous results, the electron pitch angle distributions were more anisotropic in fast wind than in slow wind. By considering the mean parameter values in fast and slow wind, we suggest that the difference in anisotropy between solar wind regimes is due almost entirely to the higher plasma densities in slow wind acting to isotropize the pitch angle distributions (see also *Ogilvie et al.* [2000]). In any solar wind region, $|\mathbf{B}|$ will dominate N in the determination of A_E , but since, on average, $|\mathbf{B}|$ is almost the same in fast and slow wind, it is unlikely that the magnetic field intensity is responsible for the observed difference in anisotropy between fast and slow wind, especially given the large difference in density between fast and slow wind.

[41] Fitting both models to fast and slow wind data for 1995 and 1996 and across energies showed that there were other significant differences between fast and slow solar wind regimes which have not been previously documented:

[42] 1. While electron number flux F_E and anisotropy A_E are equally correlated with electron heat flux in slow wind, F_E dominates substantially in fast wind.

[43] 2. Magnetic field magnitude is more dominant in determining A_E than density and dominates density more in slow wind than in fast wind.

[44] 3. Pitch angle anisotropy increases with increasing electron energy in slow wind but decreases in fast solar wind. The latter result is inconsistent with previous work by *Pilipp et al.* [1987a] and *Ogilvie et al.* [2000].

[45] 4. At the lowest suprathermal energies ($E < 200$ eV), correlation of A_E with N_p increases while correlation with $|\mathbf{B}|$ decreases.

[46] 5. The influence of density on anisotropy declines strongly with energy in fast wind but not in slow wind (Figure 12).

[47] The fits of A_E to the observed anisotropy can be used to investigate suprathermal electron scattering. *Zurbuchen et al.* [2001] showed that within plasma sheets (which they termed “magnetic holes,” see also *Crooker et al.* [2004]), the level of magnetic field fluctuations tends to be high. *Zurbuchen et al.* [2001] suggest that these fluctuations could be responsible for scattering suprathermal electrons in plasma sheets. *Mullan et al.* [2003] further show that fluctuations in magnetic field strength are anticorrelated with Alfvén speed so that maxima in magnetic field fluctuations occur during local minima in Alfvén speed. These minima will correspond to times when $|\mathbf{B}|$ is low and N_p is high (i.e., in plasma sheets). *Crooker et al.* [2004] further show that high-beta regions in the solar wind are often embedded within high-density plasma sheets and that it is a drop in the magnetic field strength that primarily controls the rise in beta. These somewhat independent behaviors of magnetic field strength and plasma density justify our treating them separately, rather than in physical parameters like plasma beta and Alfvén speed. Our results suggest that a variety of scattering processes are active in the solar wind in the different solar wind regimes.

[48] We tentatively infer that the reasonable fit of A_M using only in situ solar wind parameters provides support for the assumption that the shape of the electron pitch angle distributions is determined primarily by in situ scattering and not by solar source conditions. We also infer that the key parameter for studying the solar/coronal source of heat flux, its variability and possible magnetic field line disconnection events is the number density of hot electrons F_E [c.f. *Gosling et al.*, 2004], while A_E (or any parameterization of the pitch angle distribution anisotropy that is independent of suprathermal electron number flux) is the key parameter for analyzing local scattering of suprathermal electrons. Finally, we conclude that the excellent fit of Q_M to the observed heat flux provides substantial support for the phenomenological model of heat flux as $\mathbf{Q} \sim F_H\Delta\mathbf{V}_H$ [*Feldman et al.*, 1975; *Scime et al.*, 1994].

[49] **Acknowledgments.** C. Pagel and N. Crooker are supported by the National Science Foundation under grants ATM-0327739 and ATM-0119700. C. Pagel would also like to thank J. T. Gosling for useful discussion.

[50] Shadia Rifai Habbal thanks Earl Scime for his assistance in evaluating this paper.

References

- Cane, H. V., and I. G. Richardson (2003), Interplanetary coronal mass ejections in the near-Earth solar wind during 1996–2002, *J. Geophys. Res.*, *108*(A4), 1156, doi:10.1029/2002JA009817.
- Chisham, G., S. J. Schwartz, D. Burgess, S. D. Bale, M. W. Dunlop, and C. T. Russell (2000), Multisatellite observations of large magnetic depressions in the solar wind, *J. Geophys. Res.*, *105*, 2325–2335.
- Crooker, N. U., D. E. Larson, S. W. Kahler, S. M. Lamassa, and H. E. Spence (2003), Suprathermal electron isotropy in high-beta solar wind and its role in heat flux dropouts, *Geophys. Res. Lett.*, *30*(12), 1619, doi:10.1029/2003GL017036.
- Crooker, N. U., C.-L. Huang, S. M. Lamassa, D. E. Larson, and S. W. Kahler (2004), Heliospheric plasma sheets, *J. Geophys. Res.*, *109*, A03107, doi:10.1029/2003JA010170.
- Feldman, W. C., J. R. Asbridge, S. J. Bame, M. D. Montgomery, and S. P. Gary (1975), Solar wind electrons, *J. Geophys. Res.*, *80*, 4181–4196.
- Feldman, W. C., J. R. Asbridge, S. J. Bame, S. P. Gary, and M. D. Montgomery (1976a), Electron parameter correlations in high-speed streams and heat flux instabilities, *J. Geophys. Res.*, *81*, 2377–2382.
- Feldman, W. C., J. R. Asbridge, S. J. Bame, S. P. Gary, M. D. Montgomery, and S. M. Zink (1976b), Evidence for regulation of solar wind heat flux at 1 AU, *J. Geophys. Res.*, *81*, 5207–5210.

- Feldman, W. C., J. R. Asbridge, S. J. Bame, J. T. Gosling, and D. S. Lemons (1978), Characteristic electron variations across simple high-speed solar wind streams, *J. Geophys. Res.*, *83*, 5285–5295.
- Feldman, W. C., R. C. Anderson, J. R. Asbridge, S. J. Bame, J. T. Gosling, and R. D. Zwickl (1982), Plasma electron signature of magnetic connection to the Earth's bow shock: ISEE 3, *J. Geophys. Res.*, *87*, 632–642.
- Fisk, L. A., T. H. Zurbuchen, and N. A. Schwadron (1999), On the coronal magnetic field: Consequences of large-scale motions, *Astrophys. J.*, *521*, 868–877.
- Fitzenreiter, R. J., and K. W. Ogilvie (1992), Heat flux dropouts in the solar wind and coulomb scattering effects, *J. Geophys. Res.*, *97*, 19,213–19,219.
- Gosling, J. T., D. N. Baker, S. J. Bame, W. C. Feldman, and R. D. Zwickl (1987), Bidirectional solar wind electron heat flux events, *J. Geophys. Res.*, *92*, 8519–8535.
- Gosling, J. T., C. A. de Koning, R. M. Skoug, J. T. Steinberg, and D. J. McComas (2004), Dispersionless modulations in low-energy electron bursts and discontinuous changes in the solar wind electron strahl, *J. Geophys. Res.*, *109*, A05102, doi:10.1029/2003JA010338.
- Haggerty, D. K., E. C. Roelof, C. W. Smith, N. F. Ness, R. L. Tokar, and R. M. Skoug (2000), Interplanetary magnetic field connection to the L1 Lagrangian orbit during upstream energetic ion events, *J. Geophys. Res.*, *105*, 25,213–25,131.
- Hammond, C. M., W. C. Feldman, D. J. McComas, J. L. Phillips, and R. J. Forsyth (1996), Variation of electron-strahl width in the high-speed solar wind: Ulysses observations, *Astron. Astrophys.*, *316*, 350–354.
- Lepping, R. L., et al. (1995), The Wind magnetic field investigation, *Space Sci. Rev.*, *71*, 207–229.
- Lin, R. P., and S. W. Kahler (1992), Interplanetary magnetic field connection to the Sun during electron heat flux dropouts in the solar wind, *J. Geophys. Res.*, *97*, 8203–8209.
- Lin, R. P., et al. (1995), A three-dimensional plasma and energetic particle investigation for the WIND spacecraft, *Space Sci. Rev.*, *71*, 125–153.
- McComas, D. J., J. T. Gosling, J. L. Phillips, and S. J. Bame (1989), Electron heat flux dropouts in the solar wind: Evidence for interplanetary magnetic field reconnection?, *J. Geophys. Res.*, *94*, 6907–6916.
- Mullan, D. J., C. W. Smith, N. F. Ness, and R. M. Skoug (2003), Short-period magnetic fluctuations in Advanced Composition Explorer solar wind data: Evidence for anticorrelation with Alfvén speed, *Astrophys. J.*, *583*, 496–505.
- Ogilvie, K. W., et al. (1995), SWE, a comprehensive plasma instrument for the Wind spacecraft, *Space Sci. Rev.*, *71*, 55–77.
- Ogilvie, K. W., L. F. Burlaga, D. J. Chronay, and R. Fitzenreiter (1999), Sources of the solar wind electron strahl in 1995, *J. Geophys. Res.*, *104*, 22,389–22,393.
- Ogilvie, K. W., R. Fitzenreiter, and M. Desch (2000), Electrons in the low-density solar wind, *J. Geophys. Res.*, *105*, 27,277–27,288.
- Phillips, J. L., J. T. Gosling, D. J. McComas, S. J. Bame, and S. P. Gary (1989), Anisotropic thermal electron distributions in the solar wind, *J. Geophys. Res.*, *94*, 6563–6579.
- Pilipp, W. G., H. Miggenieder, M. S. Montgomery, K.-H. Mühläuser, H. Rosenbauer, and R. Schwenn (1987a), Characteristics of electron velocity distribution functions in the solar wind derived from the Helios plasma experiment, *J. Geophys. Res.*, *92*, 1075–1092.
- Pilipp, W. G., H. Miggenieder, K.-H. Mühläuser, H. Rosenbauer, R. Schwenn, and F. M. Neubauer (1987b), Variations of electron distribution functions in the solar wind, *J. Geophys. Res.*, *92*, 1103–1118.
- Pilipp, W. G., H. Miggenieder, K.-H. Mühläuser, H. Rosenbauer, and R. Schwenn (1990), Large-scale variations of thermal electron parameters in the solar wind between 0.3 and 1 AU, *J. Geophys. Res.*, *95*, 6305–6329.
- Scime, E. E., S. J. Bame, W. C. Feldman, S. P. Gary, J. L. Phillips, and A. Balogh (1994), Regulation of solar wind electron heat flux from 1 to 5 AU: Ulysses observations, *J. Geophys. Res.*, *99*, 23,401–23,410.
- Scime, E. E., A. Badeau Jr., and J. E. Littleton (1999), The electron heat flux in the polar solar wind: Ulysses observations, *Geophys. Res. Lett.*, *26*, 2129–2132.
- Scime, E. E., J. E. Littleton, S. P. Gary, R. Skoug, and L. Naiguo (2001), Solar cycle variations in the electron heat flux: Ulysses observations, *Geophys. Res. Lett.*, *28*, 2169–2172.
- Skoug, R. M., W. C. Feldman, J. T. Gosling, and D. J. McComas (2000), Solar wind electron characteristics inside and outside coronal mass ejections, *J. Geophys. Res.*, *105*, 23,069–23,084.
- Winterhalter, D., E. J. Smith, M. E. Burton, N. Murphy, and D. J. McComas (1994), The heliospheric plasma sheet, *J. Geophys. Res.*, *99*, 6667–6680.
- Zurbuchen, T. H., S. Hefti, L. A. Fisk, G. Gloeckler, N. A. Schwadron, C. W. Smith, N. F. Ness, R. M. Skoug, D. J. McComas, and L. F. Burlaga (2001), On the origin of microscale magnetic holes in the solar wind, *J. Geophys. Res.*, *106*, 16,001–16,010.

N. U. Crooker, M. J. Owens, and C. Pagel, Center for Space Physics, Boston University, Boston, MA 02215, USA. (pagel@bu.edu)

S. W. Kahler, Air Force Research Laboratory, Hanscom Air Force Base, MA 01731, USA.

D. E. Larson, Space Science Laboratory, University of California, Centennial at Grizzly Peak Blvd., Berkeley, CA 94720-7450, USA.